Results in Physics 14 (2019) 102462

Contents lists available at ScienceDirect

Results in Physics

journal homepage: www.elsevier.com/locate/rinp

Electromagnetic shielding via a virtual pillar with a magnetic wall

Seong-Han Kim, Chul-Sik Kee*

Integrated Optics Laboratory, Advanced Photonics Research Institute, Gwangju Institute of Science and Technology, Gwangju 61005, Republic of Korea

ARTICLE INFO

Keywords:
Electromagnetic shielding
Metamaterials
Perfect magnetic conductors

ABSTRACT

It is demonstrated that the objects enclosed by a virtual pillar with a magnetic wall can be completely shielded from EM waves through numerical simulations. The simulated total scattering cross section of a dielectric rod enclosed by a virtual pillar is identical to that of an empty virtual pillar. In addition, the simulated spatial distributions of the total fields including the incident electric field and scattered electric field from the former are similar to those from the latter. The penetration depth of electromagnetic waves into the pillar is derived as a function of the height of the pillar. A virtual pillar with an open boundary can provide an unusual electromagnetic environment.

Introduction

Electromagnetic (EM) shielding, which is done to block EM waves, is essential for isolating objects electromagnetically. In practice, EM shielding is required to protect electrical devices from their surroundings. Metal sheets and foams are usually employed to block EM waves. Recently, flexible graphene foam composites and hybrid structures of graphene and polymers have been proposed for high-performance EM interference shielding. [1,2] The potential of two-dimensional transition metal cardide/polymer composite films with good flexibility and high conductivity have been demonstrated for EM shielding.[3].

Artificial periodic structures including photonic crystals and metamaterials have been proposed to shield or hide objects from EM waves. For example, photonic crystals can block EM waves in the frequency ranges of their photonic band gaps and can hide objects at the frequency of the Dirac cone with a zero refractive index.[4,5] Metamaterials can hide objects in a quite different way. By properly designing the effective dielectric permeability and magnetic permittivity of a metamaterial to enclose an object, it is possible for EM waves to pass through the metamaterial without interacting with the object; this is known as invisible cloaking.[6,7].

Recently, it was reported that a parallel configuration perfect electric conducting (PEC) and perfect magnetic conducting (PMC) plates can give rise to a magnetic wall to block transverse EM (TEM) modes at the interface between parallel PEC and PMC plates.[8] Usually, a parallel PEC plate waveguide can support TEM modes between the plates. However, a combination of parallel PEC and PMC plate waveguides cannot support TEM modes because TEM modes propagating in a parallel PEC plate waveguide are completely reflected at the interface between parallel PEC and PMC plate waveguides. The magnetic wall is formed at the interface between parallel PEC and PMC plate waveguides.

A virtual pillar with a magnetic wall can be created inside a parallel PEC plate waveguide by introducing a circular PMC patch in the upper PEC plate of the waveguide.[8] The simulated scattering properties of a virtual pillar with a circular magnetic wall for the TEM modes of the waveguide demonstrated that a virtual pillar mimics a PMC pillar with a radius less than that of the circular PMC patch because EM waves can slightly penetrate the wall. It is expected that an object enclosed by a virtual pillar can be easily shielded from EM waves when the size of the object is smaller than the diameter of the pillar. Furthermore, since a virtual pillar has an open boundary, the pillar can provide unusual EM environments.

In this paper, it is numerically demonstrated that the objects enclosed by a virtual pillar with a magnetic wall can be completely shielded from EM waves. The simulated scattering cross section of a virtual pillar with a dielectric rod is identical to that of an empty virtual pillar, and the simulated spatial distributions of the electric fields scattered from the former and latter are similar, as well. Since the penetration depth of EM waves into the pillar increases as the height of the pillar increases, proper EM shielding depends on conditions such as the height of the pillar and the diameter of the pillar.

* Corresponding author.
E-mail address: cskee@gist.ac.kr (C.-S. Kee).

https://doi.org/10.1016/j.rinp.2019.102462
Received 19 October 2018; Received in revised form 18 June 2019; Accepted 18 June 2019
Available online 26 June 2019

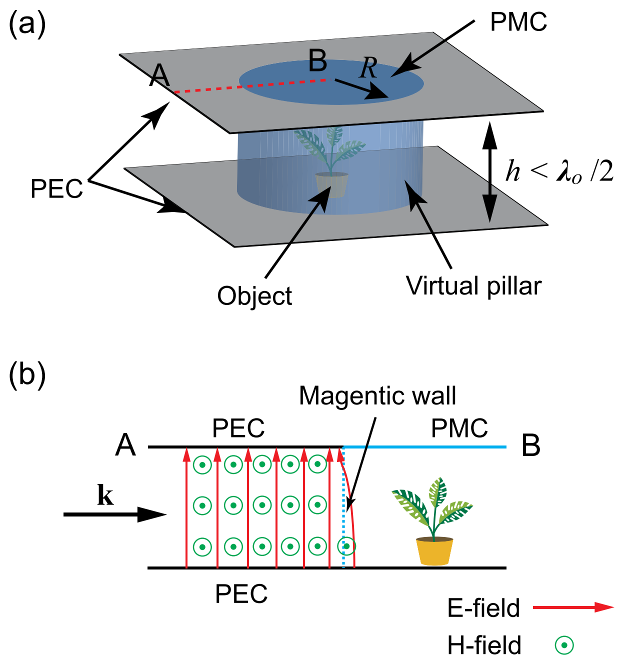

Fig. 1. (a) Schematic of the electromagnetic shielding of a vase enclosed by a virtual pillar with a magnetic wall in a parallel perfect electric conductor plate waveguide. R is the radius of the circular perfect magnetic conductor patch and h is the distance between the two perfect electric conductor plates (the height of the pillar). (b) Schematic of the field distributions of a transverse electromagnetic mode on the cross section along line A-B in (a).

Results

Fig. 1(a) shows the schematic of the EM shielding of a vase enclosed by a virtual pillar with a magnetic wall in a parallel PEC plate waveguide. R is the radius of the circular PMC patch and h is the distance between the two PEC plates (the height of the pillar). Here, h is adjusted to a value less than half the wavelength to allow only TEM modes in the waveguide. The electric fields and magnetic fields of TEM modes in a parallel plate waveguide are perpendicular and parallel to the plates, respectively, as illustrated in the schematic of field distributions of a TEM mode on the cross section along line A-B (Fig. 1(b)). Under the PMC patch, where the vase is located, there are no fields, except for fringe effects around the magnetic wall.

Prior to studying the EM shielding of the virtual pillar, the total scattering cross sections and spatial distributions of the total fields, including the incident electric fields and scattered electric fields from three different scatterers such as the square, circular, and triangular dielectric rods placed in the parallel plate waveguide, were simulated. COMSOL Multiphysics, based on a finite-element method, was employed to calculate the total scattering cross sections and field spatial distributions.

Fig. 2 (a) shows the simulated total scattering cross sections of the three different dielectric rods as a function of the frequency of the incident TEM wave when h = 0.1 cm. The radius of the circular dielectric rod r = 0.5 cm, and the square and triangular rods are inscribed in the circle. The total scattering cross sections were normalized to $2rh$. Figs. 2(b)–(d) show the spatial distributions of the total fields of the square, circular, and triangular dielectric rods at a frequency of 25 GHz, respectively. The spatial distributions of the total fields depend on the shapes of the dielectric rods.

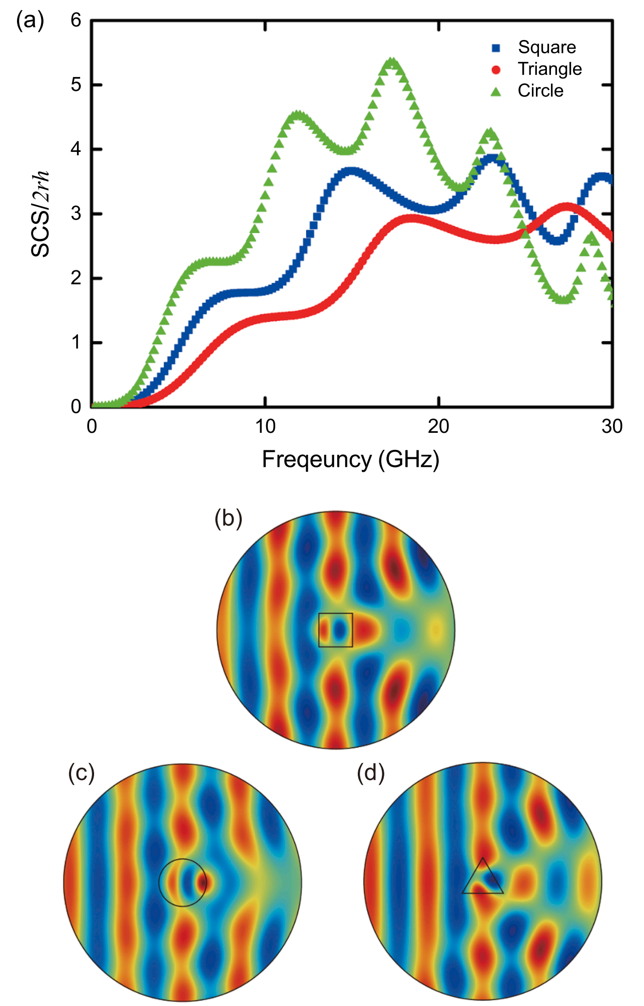

Fig. 2. (a) Simulated scattering cross sections of the square, circular, and triangular dielectric rods as a function of the frequency of the incident transverse electromagnetic wave when h = 0.1 cm. The radius of the circular dielectric rod r = 0.5 cm, and the square and triangular rods are inscribed in the circle. The total scattering cross sections were normalized to $2rh$. Spatial distributions of the total fields including the incident electric field and the scattered electric field from (b) the square, (c) circular, and (d) triangular dielectric rods at a frequency of 25 GHz. The solid square, circular, and triangular lines denote the square, circular, and triangular dielectric rods, respectively.

In order to demonstrate the EM shielding via a virtual pillar, the three different rods are placed in virtual pillars with a radius slightly larger than that of the circular rod; R = 1.25r. Fig. 3(a) shows the simulated total scattering cross sections of the three dielectric rods centered in virtual pillars and an empty virtual pillar as a function of the frequency of the incident TEM wave when h = 0.1 cm. The total scattering cross sections were normalized to $2Rh$. The simulated total scattering cross sections of the three different dielectric rods are exactly identical to that of an empty virtual pillar.

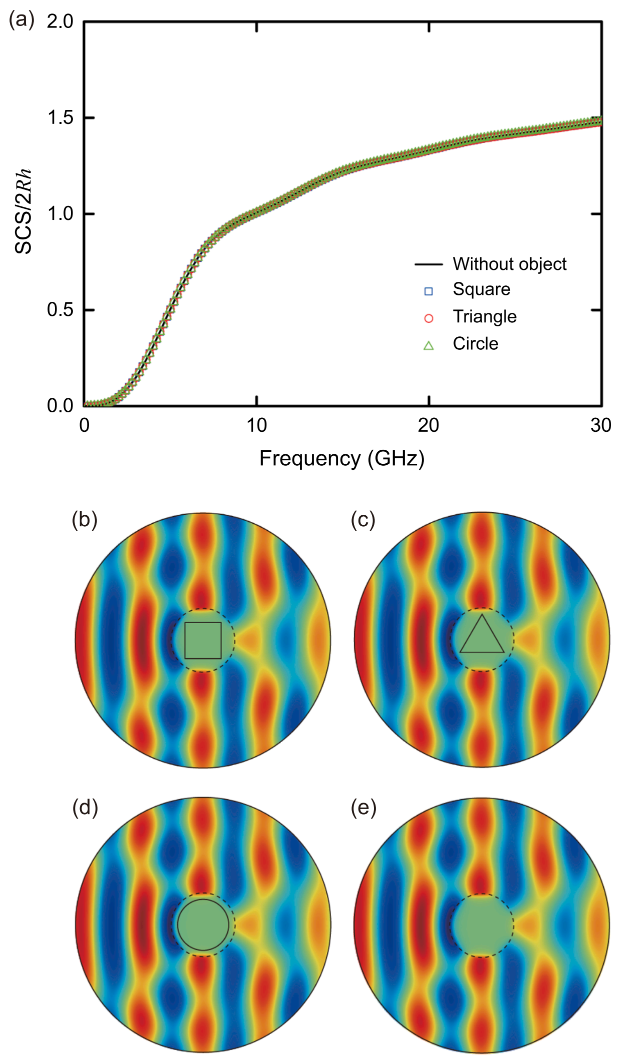

Fig. 3. (a) Simulated scattering cross sections of the virtual pillars with the square, triangular, and circular dielectric rods and an empty virtual pillar with a radius of $R = 1.25r$ as a function of the frequency of the incident transverse electromagnetic wave when $h = 0.1$ cm. The total scattering cross sections were normalized to $2Rh$. Spatial distributions of the total fields including the incident electric field and the scattered electric fields from the virtual pillars of (b) the square, (c) triangular, and (d) circular dielectric rods and (e) an empty virtual pillar at a frequency of 25 GHz. The solid square, triangular, and circular lines denote the square, triangular, and circular dielectric rods, respectively. The dashed circular line denotes the virtual wall boundary of the virtual pillar.

Figs. 3(b)–(e) show the spatial distributions of the total fields of the square, triangular, and circular dielectric rods centered in virtual pillars and an empty virtual pillar at a frequency of 25 GHz, respectively. It is clear that the spatial distributions of the total fields of the three different dielectric rods centered in virtual pillars are identical to that of the empty virtual pillar. Therefore, a virtual pillar with a virtual wall can completely shield objects from EM waves.

Fig. 4 shows the simulated total scattering cross sections of the

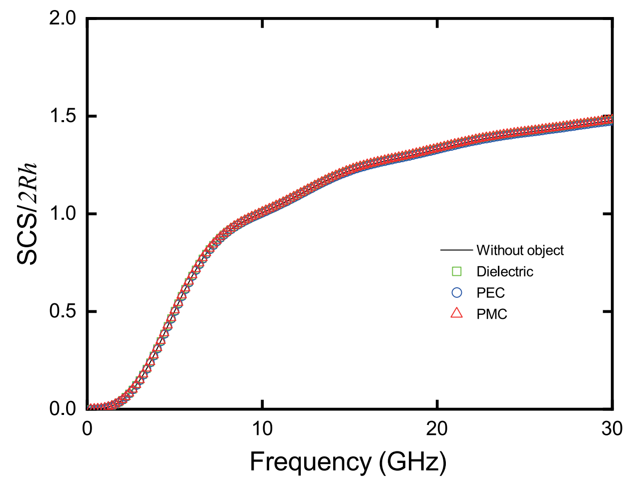

Fig. 4. Simulated scattering cross sections of the virtual pillars with the dielectric, PEC, and PMC circular rods and an empty virtual pillar with a radius of $R = 1.25r$ as a function of the frequency of the incident transverse electromagnetic wave when $h = 0.1$ cm, $r = 0.5$ cm, and $R = 1.25r$. The total scattering cross sections were normalized to $2Rh$.

dielectric, PEC, and PMC circular rods centered in virtual pillars and an empty virtual pillar as a function of the frequency of the incident TEM wave when $h = 0.1$ cm, $r = 0.5$ cm, and $R = 1.25r$. The total scattering cross sections were normalized to $2Rh$. The simulated total scattering cross sections of the three different material rods are exactly identical to that of an empty virtual pillar. The result confirms that the EM wave shielding via a virtual pillar is independent of properties of shielded materials.

Fig. 5 (a) shows the simulated magnitude of an electric field in the z-direction along the dashed line in the inset, which represents the spatial distributions of the total fields of an empty virtual pillar at a frequency of 25 GHz when h changes from 0.05 to 0.3 cm at an interval of 0.05 cm. The TEM mode penetrates the virtual pillar more deeply as h increases. Figs. 5(b)–(d) show the spatial distributions of the total fields of a virtual pillar with a square dielectric rod at a frequency of 25 GHz when $h = 0.1$, 0.2, and 0.3 cm, respectively. The spatial distributions of the total fields clearly show that the interaction between the penetrated field and the square dielectric rod becomes stronger as h increases, and the pillar does not shield the dielectric rod when $h = 0.3$ cm.

The dependence of the penetration depth z_p on h can be derived by the dispersion relation of a transverse magnetic (TM) mode of a PMC parallel plate waveguide with a width of $2h$ (see Appendix). For the lowest TM mode, $z_p = \frac{2h}{\pi}/\sqrt{1-(\frac{4h}{\lambda})^2}$, where λ is a wavelength of the TM mode. Fig. 6 shows the penetration depth estimated from Fig. 5(a) by the relation $E(z) = E_0 e^{-z/z_p}$ (square dots) and the theoretical d_p derived from the dispersion relation (solid line). They are in excellent agreement. In a long wavelength range ($\lambda \gg h$), the penetration depth is linearly proportional to h ($z_p \approx 2h/\pi$).

Fig. 7 shows the simulated total scattering cross sections of a dielectric rhombic rod centered in a virtual rhombic pillar and an empty virtual rhombic pillar as a function of the frequency of the incident TEM wave when $h = 0.1$ cm, $d = 0.53$ cm, and $\sqrt{2}D = R(R = 0.625)$ cm,

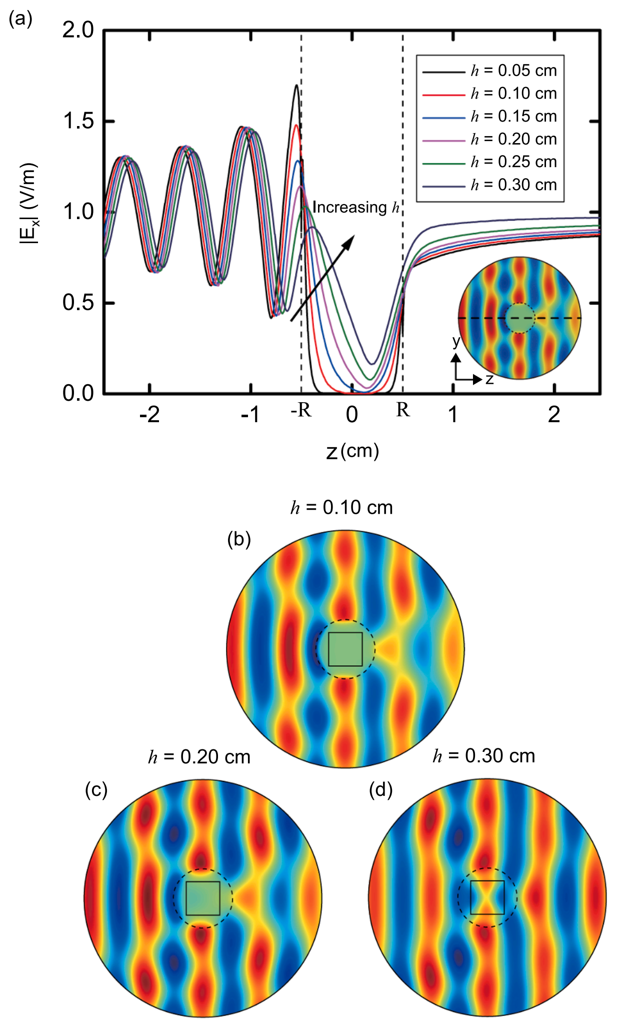

Fig. 5. (a) Simulated magnitude of an electric field in the z-direction along the dashed line shown in the inset to represent the spatial distributions of the total fields of an empty virtual pillar at a frequency of 25 GHz when h changes from 0.05 to 3.0 cm at an interval of 0.05 cm. The penetration depth of the electric field increases as h increases. The spatial simulated distributions of the total fields of a virtual pillar with a square dielectric rod at a frequency of 25 GHz when (b) $h = 0.1$, (c) 0.2, and (d) 0.3 cm.

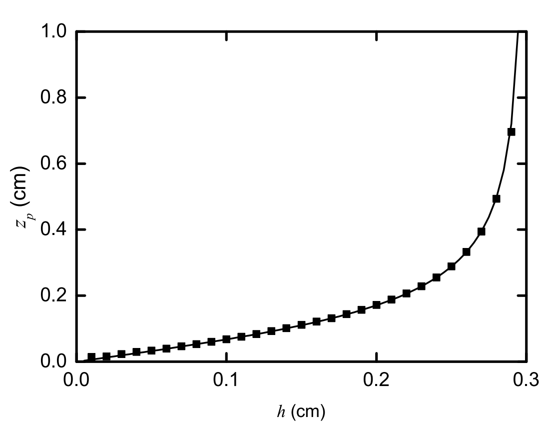

Fig. 6. Dependence of the estimated (square dots) and theoretical z_p (solid line) on h.

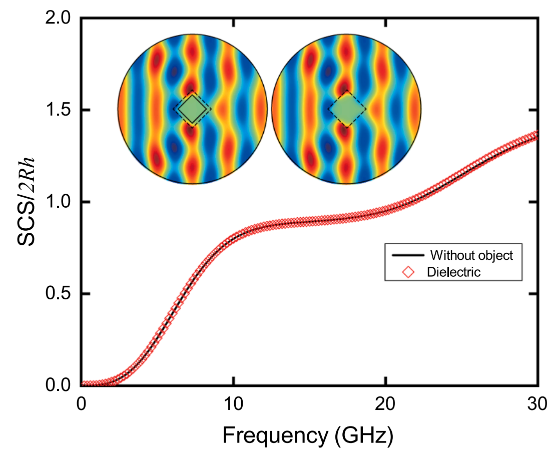

Fig. 7. Simulated total scattering cross sections of a dielectric rhombic rod centered in a virtual rhombic pillar and an empty virtual rhombic pillar as a function of the frequency of the incident TEM wave when $h = 0.1$ cm, $d = 0.53$ cm, and $\sqrt{2}D = R(R = 0.625)$ cm, where d and D are the lengthes of sides of a dielectric rhombic rod and virtual rhombic pillar, respectively. The total scattering cross sections were normalized to $2Rh$. The inset shows the spatial distributions of the total fields of a virtual rhombic pillars with a rhombic dielectric rod and an empty virtual rhombic pillar at a frequency of 25 GHz.

where d and D are the lengthes of sides of the dielectric rhombic rod and virtual rhombic pillar, respectively. The total scattering cross sections were normalized to $2Rh$. The simulated total scattering cross section of a dielectric rhombic rod is exactly identical to that of an empty virtual rhombic pillar. The result confirms that the EM wave shielding via a virtual pillar is independent of the shape of the pillar. The inset shows the spatial distributions of the total fields of a virtual pillars with a rhombic dielectric rod and an empty virtual rhombic pillar at a frequency of 25 GHz.

It should be emphasized that a virtual pillar has an open boundary in the lateral plane (yz plane). Particles and other waves excluding EM waves can pass through a virtual pillar freely. So, a virtual pillar may provide unusual EM environments. For example, an atom to emit radiation with a long wavelength freely enter inside a virtual pillar but radiation emitted from atoms can be trapped in the pillar. The trapped radiation can easily release from the pillar by increasing the height of the pillar. So, possible applications of a virtual pillar might be interesting.

Conclusion

In conclusion, it was numerically demonstrated that a virtual pillar with a magnetic wall could shield an object from EM waves by showing that the simulated total scattering cross section and the simulated spatial distribution of the total fields of a virtual pillar with a dielectric rod are identical to those of an empty virtual pillar. Since the penetration depth of EM waves into a pillar increases as the height of the pillar increases, it is possible to achieve the EM shielding via a virtual pillar under the proper conditions. A virtual pillar with a open boundary can provide unusual EM environments.

Acknowledgments

This work was supported by the Gwangju Institute of Science and Technology (GIST) Research Institute (GRI) in 2019 and the Basic

Science Research Program through the National Research Foundation of Korea (NRF) funded by the Ministry of Education, Science and Technology (Nos. 2018R1D1A1B07050116, 2017R1A2B1007631, and 2015R1D1A1A01060180).

Appendix: Transverse magnetic modes of a parallel PMC waveguide

For the z component of an electric field of a transverse magnetic (TM) mode ($H_x = 0$, $H_y \neq 0$, $H_z = 0$, $E_x \neq 0$, $E_y = 0$, and $E_z \neq 0$) of a parallel PMC plate waveguide, $E_z(x, z, t) = e_z(x)\exp[i(\beta z - \omega t)]$,

$$\left(\frac{\partial^2}{\partial x^2} + k_c^2\right)e_z(x) = 0, \tag{1}$$

where $k_c = \sqrt{\mu \epsilon \omega^2 - \beta^2}$. The general solution of Eq. (1) is $e_z(x) = A\sin(k_c x) + B\cos(k_c x)$. When the distance between the two PMC plates is $2h$, the boundary conditions of $\partial e_z(x)/\partial x = 0$ at $x = 0$ and $2h$ give that $A = 0$ and $k_c = n\pi/2h(n = 1, 2, 3\cdots)$. So, the non zero components of the TM mode are below,

$$H_y = \frac{i \epsilon \omega}{k_c}B_n\sin\left(\frac{n\pi}{2h}x\right)\exp[i(\beta z - \omega t)], \tag{2}$$

$$E_x = \frac{-i\beta}{k_c}B_n\sin\left(\frac{n\pi}{2h}x\right)\exp[i(\beta z - \omega t)], \tag{3}$$

$$E_z = B_n\cos\left(\frac{n\pi}{2h}x\right)\exp[i(\beta z - \omega t)]. \tag{4}$$

when $\mu \epsilon \omega^2 < k_c^2$ (that is,), there is no TM mode propagating in the waveguide. The non zero components of the decay mode are below,

$$H_y = \frac{i \epsilon \omega}{k_c}B_n\sin\left(\frac{n\pi}{2h}x\right)\exp(-\alpha z)\exp(-i\omega t), \tag{5}$$

$$E_x = \frac{\alpha}{k_c}B_n\sin\left(\frac{n\pi}{2h}x\right)\exp(-\alpha z)\exp(-i\omega t), \tag{6}$$

$$E_z = B_n\cos\left(\frac{n\pi}{2h}x\right)\exp(-\alpha z)\exp(-i\omega t), \tag{7}$$

where $\alpha = \sqrt{k_c^2 - \mu \epsilon \omega^2}$. The penetration depth $z_p$defined as $1/\alpha$ is

$$z_p = 1/\sqrt{\left(\frac{n\pi}{2h}\right)^2 - \left(\frac{2\pi}{\lambda}\right)^2} = \frac{2h}{\pi}/\sqrt{n^2 - \left(\frac{4h}{\lambda}\right)^2}. \tag{8}$$

The theoretical z_p shows that the penetration depth is linearly proportional to h ($z_p \approx 2h/n\pi$) when the wavelengths of TM modes are much larger than the distance between the two PMC plates ($\lambda \gg 2h$) and decreases as the order of the mode increases.

Appendix A. Supplementary data

Supplementary data associated with this article can be found, in the online version, athttps://doi.org/10.1016/j.rinp.2019.102462.

References

[1] Chen Z, Xu C, Ma C, Ren W, Cheng HM. Lightweight and flexible graphene foam composites for high-performance electromagnetic interference shielding. Adv Mater 2013;25:1296–300.
[2] Yan DX, Pang H, Li B, Vajtai R, Xu L, Ren PG, et al. Structured reduced graphene oxide/polymer composites for ultra-efficient electromagnetic interference shielding. Adv Funct Mater 2015;25:559–66.
[3] Shahzad F, Alhabeb M, Hatter CB, Anasori B, Hong SM, Koo CM, et al. Electromagnetic interference shielding with 2D transition metal carbides (MXenes). Science 2016;353:1137–40.
[4] Komarevskiy N, Shklover V, Braginsky L, Hafner C, Lawson J. Potential of glassy carbon and silicon carbide photonic structures as electromagnetic radiation shields for atmospheric re-entry. Opt Express 2012;20:14189.
[5] Huang X, Lai Y, Hang ZH, Zheng H, Chan CT. Dirac cones induced by accidental degeneracy in photonic crystals and zero-refractive-index materials. Nat Mater 2011;10:582–6.
[6] Schurig D, Mock JJ, Justice BJ, Cummer SA, Pendry JB, Starr AF, et al. Metamaterial electromagnetic cloak at microwave frequencies. Science 2006;314:977–80.
[7] Alitalo P, Tretyakov S. Electromagnetic cloaking with metamaterials. Mater Today 2009;12:22–9.
[8] Kim SH, Kim S, Kee CS. Photonic crystals composed of virtual pillars with magnetic walls: photonic band gaps and double dirac cones. Phys Rev B 2016;94:085118.